Auger Radiopharmaceutical Therapy Targeting Prostate-Specific Membrane Antigen

Ana P. Kiess[1], Il Minn*[2], Ying Chen*[2], Robert Hobbs[1], George Sgouros[1,2], Ronnie C. Mease[2], Mrudula Pullambhatla[2], Colette J. Shen[1], Catherine A. Foss[2], and Martin G. Pomper[1,2]

[1]Department of Radiation Oncology and Molecular Radiation Sciences, Johns Hopkins University, Baltimore, Maryland; and [2]Russell H. Morgan Department of Radiology and Radiological Sciences, Johns Hopkins University, Baltimore, Maryland

Auger electron emitters such as ^{125}I have a high linear energy transfer and short range of emission (<10 μm), making them suitable for treating micrometastases while sparing normal tissues. We used a highly specific small molecule targeting the prostate-specific membrane antigen (PSMA) to deliver ^{125}I to prostate cancer cells. **Methods:** The PSMA-targeting Auger emitter 2-[3-[1-carboxy-5-(4-^{125}I-iodo-benzoylamino)-pentyl]-ureido]-pentanedioic acid (^{125}I-DCIBzL) was synthesized. DNA damage (via phosphorylated H2A histone family member X staining) and clonogenic survival were tested in PSMA-positive (PSMA+) PC3 PIP and PSMA-negative (PSMA−) PC3 flu human prostate cancer cells after treatment with ^{125}I-DCIBzL. Subcellular drug distribution was assessed with confocal microscopy using a related fluorescent PSMA-targeting compound YC-36. In vivo antitumor efficacy was tested in nude mice bearing PSMA+ PC3 PIP or PSMA− PC3 flu flank xenografts. Animals were administered (intravenously) 111 MBq (3 mCi) of ^{125}I-DCIBzL, 111 MBq (3 mCi) of ^{125}I-NaI, an equivalent amount of nonradiolabeled DCIBzL, or saline. **Results:** After treatment with ^{125}I-DCIBzL, PSMA+ PC3 PIP cells exhibited increased DNA damage and decreased clonogenic survival when compared with PSMA– PC3 flu cells. Confocal microscopy of YC-36 showed drug distribution in the perinuclear area and plasma membrane. Animals bearing PSMA+ PC3 PIP tumors had significant tumor growth delay after treatment with ^{125}I-DCIBzL, with only 1 mouse reaching 5 times the initial tumor volume by 60 d after treatment, compared with a median time to 5 times volume of less than 15 d for PSMA– PC3 flu tumors and all other treatment groups (P = 0.002 by log-rank test). **Conclusion:** PSMA-targeted radiopharmaceutical therapy with the Auger emitter ^{125}I-DCIBzL yielded highly specific antitumor efficacy in vivo, suggesting promise for treatment of prostate cancer micrometastases.

Key Words: Auger; radiopharmaceutical therapy; PSMA; prostate cancer; radiotherapy; iodine

J Nucl Med 2015; 56:1401–1407
DOI: 10.2967/jnumed.115.155929

Only 4% of the more than 240,000 men in the United States who present with prostate cancer (PC) annually will have gross metastases at diagnosis (*1,2*). Nevertheless, approximately 10% will have micrometastatic disease and will eventually develop metastases after completing definitive treatment (*3,4*). There are limited therapeutic options for metastatic PC, and aside from androgen-deprivation therapy these have shown only modest survival benefits. Recent success with the α-particle emitter $^{223}RaCl_2$ for patients with metastatic PC demonstrates the potential for systemic radiopharmaceutical therapy (RPT) to improve survival with limited toxicity (*5*). Unlike $^{223}RaCl_2$, which is limited to treatment of bone metastases, we investigated Auger electron–emitting RPT that targets the prostate-specific membrane antigen (PSMA) for treatment of micrometastases in bone as well as lymph nodes and other soft tissues.

Auger emitters such as ^{125}I have greater linear energy transfer and cause more DNA damage than traditional x-rays or β-particle emitters (e.g., ^{131}I) (*6*). The short range (<10 μm) of Auger electrons is well suited for treatment of micrometastases with sparing of nearby normal tissues. However, the challenge is to target cancer cells specifically and achieve intracellular uptake for maximum DNA damage (*7*). PSMA is overexpressed 1,000-fold on the surface of PC cells, and we have developed a highly specific small-molecule Auger emitter targeting PSMA, 2-[3-[1-carboxy-5-(4-^{125}I-iodo-benzoylamino)-pentyl]-ureido]-pentanedioic acid, or ^{125}I-DCIBzL (*8–10*). Other radiolabeled ureas similar to ^{125}I-DCIBzL have been safely administered to human subjects for imaging of PC (*11,12*). ^{125}I-DCIBzL was chosen over other urea-based candidates because of sustained tumor uptake for at least 48 h in human PC xenografts (*8*). We expect that these small molecules are more able to overcome barriers to solid tumor drug delivery than larger molecules, including antibodies. Given the potential of ^{125}I-DCIBzL for RPT, we have tested its PSMA-specific uptake and cytotoxicity in vitro as well as its antitumor efficacy in vivo in a human PC xenograft model.

MATERIALS AND METHODS

Chemistry

Methods have been previously described for the synthesis of ^{125}I-DCIBzL (Fig. 1A) (*8*). This compound has demonstrated high PSMA binding affinity, with a low K_i (inhibitory constant) of 0.01 nM (*8*). For this study, the specific radioactivity for each synthesis was greater than 44.4 GBq/μmol (1,200 Ci/mmol). Methods for synthesis of the fluorescent PSMA-targeting analog 1-(3-carboxy-4-(3-hydroxy-6-oxo-6H-xanthen-9-yl)phenylamino)-9,16,24-trioxo-1-thioxo-2,8,17,23,25-pentaazaoctacosane-7,22,26,28-tetracarboxylic acid (YC-36; Fig. 1B), used for microscopy, are included in the supplemental materials (available at http://jnm.snmjournals.org).

In Vitro Studies

Isogenic PC3 PIP (PSMA-positive [PSMA+]) and PC3 flu (PSMA-negative [PSMA−]) PC cell lines were obtained from Dr. Warren Heston

Received Feb. 13, 2015; revision accepted Jun. 29, 2015.
For correspondence or reprints contact: Ana P. Kiess, Department of Radiation Oncology and Molecular Radiation Sciences, Johns Hopkins University, 401 North Broadway, Ste. 1440, Baltimore, MD 21231.
E-mail: akiess1@jhmi.edu
*Contributed equally to this work.
Published online Jul. 16, 2015.

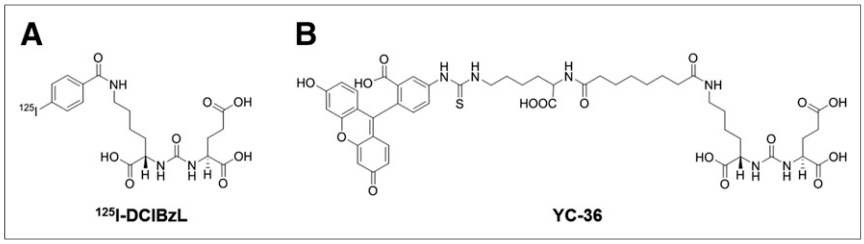

FIGURE 1. Chemical structures of ^{125}I-DCIBzL and YC-36.

(Cleveland Clinic) and maintained as previously described (*13*). The PC3 cell line was originally derived from a human PC bone metastasis and was androgen-independent (*14,15*). The PSMA+ PC3 PIP line was stably transfected to overexpress PSMA (*13*). To measure the number of PSMA binding sites on these cell lines, a radiometric binding saturation assay was performed as previously described (*16,17*). The human PC cell line LNCaP was also measured for comparison, as this line is not engineered to overexpress PSMA. Briefly, for each cell line, 10^5 cells were seeded in 24-well culture plates and incubated for 4 h at 4°C with an excess (3.7 MBq/mL [100 μCi/mL]) of ^{125}I-DCIBzL, with or without pretreatment with an excess of nonradiolabeled DCIBzL for blocking (to assess nonspecific binding). Cells were washed and detached, and the cell numbers were counted. The PSMA-specific uptake was quantified using a γ counter (1282 Compugamma CS; Pharmacia/LKB Nuclear) and converted to number of PSMA binding sites per cell using the specific activity of ^{125}I-DCIBzL.

To test cellular drug uptake, 10^5 PC3 cells (PIP or flu) were seeded in 24-well culture plates. The test compounds were diluted in prewarmed medium at different concentrations (0, 3.7, 18.5, 37, and 370 kBq/mL) and incubated with the cells for 18 h at 37°C. For blocking studies (to assess nonspecific uptake), medium also contained an excess (1 μM) of nonradiolabeled DCIBzL. After incubation, cells were washed to remove extracellular DCIBzL, detached, and counted, as previously described (*18*). Cellular radioactivity was quantified using a γ counter.

For determination of subcellular localization of PSMA-targeting compounds, we used the fluorescent-labeled compound YC-36 that has the same PSMA-binding urea scaffold as DCIBzL. Previously published reports by Chen et al. have shown that these small-molecule optical agents have high PSMA binding affinity and targeted uptake in PSMA+ PC3 PIP tumors for at least 24 h, similar to DCIBzL (*19,20*). Cells (10^4) were plated onto 8-well chamber slides and incubated at 37°C for 1 d. Cells were incubated with the fluorescent PSMA compound YC-36 for 1 h at 37°C, then washed and fixed with formalin. Thirty Z stacks of confocal images were taken at 0.05-μm intervals using a Nikon A1 Confocal system (Nikon Instruments). Fluorescent pixel values were measured from each cell (n = 15) for the entire cell, the plasma membrane, and the perinuclear area using Image J software (National Institutes of Health). Other intracellular distribution was calculated by subtracting the values of plasma membrane and perinuclear area from that of the entire cell. This was performed in PSMA+ PC3 PIP cells but not PSMA– PC3 flu cells because previous fluorescence-activated cell sorting after staining with YC-36 showed that no PC3 flu cells stained with any detectable intensity (supplemental materials).

To assess DNA damage (double-strand breaks) after ^{125}I-DCIBzL treatment, staining for phosphorylated H2A histone family member X (γH2AX) was performed. Cells (10^4) were plated onto 8-well chamber slides and incubated at 37°C for 1 d. Cells were incubated with different concentrations of ^{125}I-DCIBzL (0, 3.7, 18.5, 37, and 370 kBq/mL) for 18 h in medium at 37°C, with or without an excess of nonradiolabeled DCIBzL for blocking (n = 3 wells per treatment group). After washing, fixing, and blocking, they were incubated with mouse anti-phospho-histone H2AX (Ser139) antibody at 1:1,000 for 1 h (EMD Millipore), Alexafluor 488 goat anti-mouse IgG at 1:500 for 1 h (Molecular Probes), and Hoechst 33342 dye at 1:1,000 for 2 min (Molecular Probes). Images were captured from 3 high-power (40×) fields per well using a Nikon 80i epifluorescence microscope, and γH2AX foci and the number of cells were counted per high-power field (*21*).

In vitro cell survival was tested using the clonogenic survival assay. Cells (200–1,000) were seeded in 60-mm culture dishes. The test compounds were diluted in prewarmed medium at different concentrations (0, 3.7, 18.5, 37, and 370 kBq/mL) and incubated with the cells for 18 h. The radiolabeled compound was replaced with fresh medium, and cells were incubated for 2 wk or until colonies had at least 50 cells. The colonies were stained with crystal violet and counted, and the surviving fraction was normalized to the control plating efficiency (*22*).

Dosimetry

Absorbed doses to the cell nuclei for each time point were calculated as the sum of contributions from individual cell Auger and photon emissions and the Petri dish-wide photon emissions. The cellular activity per cell and the distribution (cytoplasm vs. cell membrane vs. perinuclear) were determined from the drug uptake and distribution studies. The activity was assumed to decay only by physical decay, and the time-integrated activity (or number of events) was determined by integrating to the 14-d time point for the cellular decays and to 18 h for the photon background. The cell dosimetry was modeled using GEANT4 Monte Carlo simulations, a software package developed by the European Organization for Nuclear Research (*23*). Cells were modeled with a diameter of 26 μm and nuclear diameter of 18 μm based on median measurements from 100 PSMA+ PC3 PIP cells. From these simulations, absorbed fractions of dose to the nucleus from the cellular ^{125}I Augers in 3 different configurations (cell membrane, cytoplasm, perinuclear) were calculated and then weighted per the activity distribution results.

In Vivo Studies

All animal studies were undertaken in compliance with and approval of the Johns Hopkins Animal Care and Use Committee. Male athymic nude mice (Charles River Laboratories) were used at 8 wk of age (20 g). The maximum-tolerated dose was defined as the highest dose at which no animal died or lost more than 20% of its initial treatment weight. Treatment was administered as a single intravenous dose of ^{125}I-DCIBzL, with doses of 3.7, 18.5, 37, and 111 MBq (0.1, 0.5, 1 and 3 mCi; n = 3 mice per dose), and animals were then weighed and inspected twice per week for 60 d. As PSMA-targeted RPT would be most likely to affect kidney and hematologic function, serum creatinine and complete blood counts were measured at 4 d after injection (*9*).

In vivo antitumor efficacy was assessed using a flank xenograft tumor growth delay model. Cells were grown to 80%–90% confluence before trypsinization and formulation in RPMI for implantation into mice. Male nude mice were injected subcutaneously in the flank area with 1×10^6 PSMA+ PC3 PIP or PSMA– PC3 flu cells. Treatments were administered 7–10 d later when tumor diameter was only 3–4 mm, to mimic micrometastases. Animals were treated with a single intravenous dose of 111 MBq (3 mCi) of ^{125}I-DCIBzL, 111 MBq (3 mCi) of ^{125}I- sodium iodide, an equivalent amount of nonradiolabeled DCIBzL, or saline. The equivalent molar amount of nonradiolabeled DCIBzL was calculated using the specific molar activity of ^{125}I-DCIBzL. Animals receiving ^{125}I-NaI were pretreated with potassium iodide in their water to block thyroid uptake. The tumors were then

measured 3 times per week until they reached 5 times the initial treatment volume or 60 d. To minimize error, we used high-resolution calipers and the same author, who was masked to the treatment group information, for all measurements. The probability of reaching 5 times the initial tumor volume was characterized using Kaplan–Meier curves, and comparison was performed using the log-rank test. In addition, we conducted SPECT/CT at 24 h after treatment with ^{125}I-DCIBzL in 2 mice bearing PSMA+ PC3 PIP and 2 mice bearing PSMA– PC3 flu to confirm PSMA-specific tumor uptake (supplemental methods).

RESULTS

In Vitro Studies

Using confocal microscopy to assess subcellular drug distribution, we observed that YC-36 (Fig. 1) was localized to the perinuclear area as well as the plasma membrane. Figure 2 shows subcellular drug distribution after treatment of PSMA+ PC3 PIP cells stained with YC-36 for 1 h (n = 15). Approximately 14% (±0.7% SEM) of the total cellular drug was localized to the perinuclear area, in 1 or 2 discrete foci per cell. As discussed below, those foci may represent the mitotic spindle poles or recycling endosomal compartment. Given the short range of Auger electrons, such perinuclear localization has important implications for the potential of ^{125}I-DCIBzL to cause DNA damage (Fig. 1).

We determined the number of PSMA binding sites on cells using a radiometric binding saturation assay (*16,17*). The mean number of PSMA binding sites was 4.9×10^6 sites/cell for PC3 PIP cells and 2.5×10^3 sites/cell for PC3 flu cells. In comparison, LNCaP had 5.9×10^5 sites/cell, less than 1 order of magnitude lower than PC3 PIP. Drug uptake of ^{125}I-DCIBzL in PSMA+ PC3 PIP cells was significantly higher than in PSMA– PC3 flu cells and increased linearly with extracellular drug concentration (Fig. 3A). When blocked with a nonradiolabeled excess of DCIBzL, there was minimal nonspecific uptake of ^{125}I-DCIBzL in either cell line. Those results are consistent with the high PSMA binding affinity (K_i = 0.01nM) of ^{125}I-DCIBzL (*8*).

To measure cellular damage caused by the Auger electrons from ^{125}I-DCIBzL, we quantified double-strand DNA breaks by counting γH2AX foci per cell in 3 high-resolution fields from each of 3 wells per treatment group. As shown in Figure 3B (and Supplemental Fig. 2), the extent of DNA damage after treatment with ^{125}I-DCIBzL in PSMA+ PC3 PIP cells was significantly higher than that in PSMA– PC3 flu cells. The number of γH2AX foci per cell increased in a dose-dependent manner only in PSMA+ PC3 PIP cells, indicating PMSA-targeted localization of ^{125}I-DCIBzL (Fig. 3B). The lack of DNA damage over baseline seen in PSMA– PC3 flu cells is consistent with the high specificity of DCIBzL for PSMA. Furthermore, in the control groups, exposure to the highest extracellular concentration of ^{125}I-DCIBzL (370 kBq/mL) for 18 h still did not result in significant DNA damage, suggesting that specific uptake and proximity of ^{125}I to the nucleus is important.

The in vitro clonogenic survival assay showed a significant decrease in surviving fraction in PSMA+ PC3 PIP cells after treatment with ^{125}I-DCIBzL when compared with PSMA– PC3 flu cells (Fig. 4A). These results mirror those seen above for PSMA-specific drug uptake and DNA damage in PSMA+ PC3 PIP cells. Cells treated with an equivalent molar amount of nonradiolabeled DCIBzL showed only a mild decrease in surviving fraction, suggesting that the PSMA-targeting scaffold itself did not have cytotoxic activity. The curve of surviving fraction for PSMA+ PC3 PIP cells is roughly an exponential function of extracellular drug concentration. However, when that was modeled using Monte Carlo simulations as a function of estimated dose to the nucleus, it was not perfectly linear on a logarithmic scale (Fig. 4B), as would have been expected for Auger electrons, which may be due to overestimation of the highest dose to the nucleus (~50 Gy), as discussed below. Note also that the cellular dose was almost entirely due to the cellular Auger emissions; the contribution from the background photons was consistently on the order of 0.01%. This is essentially due to the small size of the cellular nucleus compared with the Petri dish and the short period of time that the background decays are present (18 h), which more than compensate for the fact that the photon energy per decay is greater (42 keV) than the fraction of Auger energy deposited in the cells from ^{125}I located on the nuclear surface (6.7 keV), in the cytoplasm (1.5 keV), or on the cell surface (0.84 keV).

In Vivo Studies

In our in vivo ^{125}I-DCIBzL dose-escalation study, no animal died at any dose level from 3.7 (0.1 mCi) to 111 MBq (3 mCi) (n = 3 mice per dose level). Therefore, the maximum-tolerated dose of ^{125}I-DCIBzL may be greater than 111 MBq (3 mCi) in mice, which is roughly equivalent to 296 GBq (8 Ci) in humans, but this is near the upper limit that is clinically feasible to administer from a radiation safety perspective. PSMA is known to be expressed in the renal proximal tubules, and our previously published biodistribution data for ^{125}I-DCIBzL showed tumor-to-kidney ratios of 0.1 for up to 48 h (*8*). Therefore, we measured serum creatinine in the treated mice and 3 control mice at 4 d after injection for kidney toxicity. All animals tested had normal creatinine values (0.2–0.4 mg/dL). We also measured hematologic function with complete blood counts at 4 d after injection, and these showed mild elevation in neutrophil count (up to 4.42 K/μL after 111 MBq [3 mCi]; control, 1.89–2.11 K/μL) and eosinophil count (up to 0.28 K/μL after 111 MBq [3 mCi]; control, 0.05–0.07 K/μL), possibly indicating a mild acute inflammatory reaction. These acute toxicity and survival data were used to select a dose (111 MBq [3 mCi]) for further in vivo studies, but as noted below, they do not assess the dose-limiting late toxicities that may occur 6–12 mo after treatment.

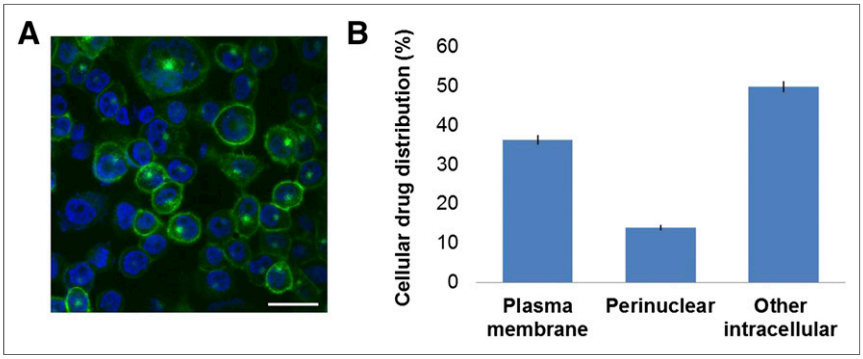

FIGURE 2. Subcellular distribution of YC-36 in PSMA+ PC3 PIP cells. Confocal microscopic images (A) and quantified regional intensity (B) show localization to perinuclear area and cell membrane. Scale bar indicates 10 μm, and error bars indicate SEM (n = 15).

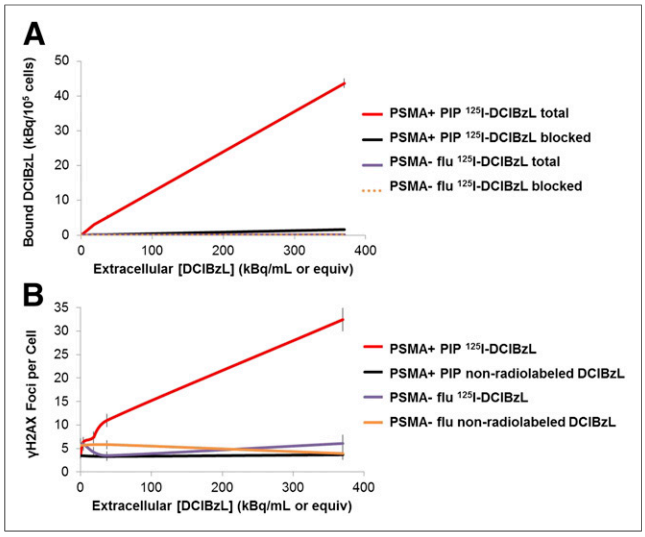

FIGURE 3. Cellular drug uptake (A) and DNA damage (B) after treatment with ^{125}I-DCIBzL in PSMA+ PC3 PIP cells or PSMA– PC3 flu cells. Error bars indicate SEM (n = 3/time point).

Nude mice bearing PSMA+ PC3 PIP tumors had significant tumor growth delay after treatment with 111 MBq (3 mCi) of ^{125}I-DCIBzL, with only 1 animal reaching 5 times the initial tumor volume by 60 d after treatment, compared with a median time to 5 times tumor volume of less than 15 d for PSMA– PC3 flu tumors and all other treatment groups (Fig. 5A; n = 5 mice per group). The difference among treatment groups was statistically significant (P = 0.002) by the log-rank test. Individual tumor volume measurements for each animal are shown in Supplemental Figure 3. There was also a mild treatment benefit seen in animals treated with 111 MBq (3 mCi) of ^{125}I-NaI, but there was no significant difference for this group nor any others besides the PSMA+ PIP group treated with ^{125}I-DCIBzL. There was no treatment benefit seen in animals treated with nonradiolabeled DCIBzL, again suggesting that the PSMA-targeting scaffold does not contribute significantly to the efficacy of ^{125}I-DCIBzL. SPECT/CT images (Fig. 5B) at 24 h after treatment with ^{125}I-DCIBzL confirmed uptake in the PSMA+ PC3 PIP tumors (left) but not in the PSMA– PC3 flu tumors (right), as expected. There was also uptake in the kidneys and thyroid gland, as discussed below.

DISCUSSION

We have investigated a novel Auger electron–based RPT targeting PSMA. The compound was delivered not only to the cell membrane but also to the perinuclear area of PSMA-expressing PC cells. Treatment with ^{125}I-DCIBzL resulted in PSMA-specific DNA damage and decreased clonogenic survival in vitro. Finally, ^{125}I-DCIBzL demonstrated excellent antitumor efficacy in vivo in mice bearing PSMA+ human PC xenografts, with only 1 animal reaching 5 times the initial tumor volume by 60 d after treatment, a significant tumor growth delay compared with PSMA– tumors and all other control groups (P = 0.002).

This is one of the few studies to demonstrate antitumor efficacy after systemic administration of an Auger RPT. Auger emitters are recognized to have potential advantages for treatment of micrometastatic cancer, including higher linear energy transfer and much shorter range (<10 μm) than β emitters or x-rays (*6,7,24–27*), though β emitters are likely to remain more effective for treatment of macroscopic disease. The potential for Auger emitter therapy was confirmed by our results, with sustained tumor responses for at least 60 d in treated animals, likely due in part to the high PSMA affinity of ^{125}I-DCIBzL, enabling sustained tumor sequestration, and the long physical half-life of ^{125}I of 59 d, which provides continuous exposure and resulting DNA damage. In addition, the dose-escalation study showed no animal deaths, weight loss, or renal or hematologic toxicity at any dose up to 111 MBq (3 mCi) at the time points assessed. However, given kidney uptake of ^{125}I-DCIBzL, late toxicity data up to 1 y after treatment are required to assess for potential nephrotoxicity.

With the short range of Auger electrons, a major challenge is to achieve close proximity to DNA to cause strand breaks. Using confocal microscopy with a fluorescent analog of DCIBzL, we showed that this agent was localized not only to the plasma membrane but also to the perinuclear area of PSMA-expressing cells, in 1 or 2 discrete foci per cell (Fig. 2A). Previous studies have shown that PSMA is internalized via a clathrin-dependent endocytic mechanism and may then be localized to the recycling endosomal compartment (*28*). Recent work by Rajasekaran et al. suggests that PSMA is specifically localized to the mitotic spindle poles, associating with the anaphase-promoting complex and possibly inducing aneuploidy in PC cells (*29*). The discrete perinuclear foci that we have observed are consistent with localization to the mitotic spindle poles, which would bring the Auger emitter close to DNA during mitosis, especially in anaphase when the condensed chromosomes are pulled toward the spindle poles. Proximity is critical for direct DNA damage because, though ^{125}I emits approximately 20 Auger electrons per decay, most of these have a range of less than 1 μm (*30*). This provides an additional layer of cancer specificity for ^{125}I-DCIBzL, as the close vicinity between the spindle poles and chromosomes would occur only in actively dividing tumors. This may effectively spare the kidney,

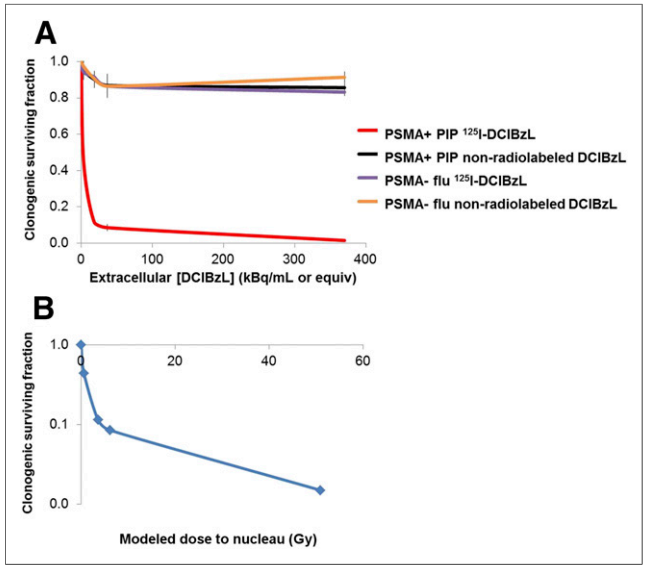

FIGURE 4. (A) Cellular clonogenic survival after treatment with ^{125}I-DCIBzL in PSMA+ PC3 PIP cells or PSMA– PC3 flu cells. Error bars indicate SEM (n = 3/time point). (B) Clonogenic survival plotted as logarithmic function of Monte Carlo modeled nuclear dose in PSMA+ PC3 PIP cells.

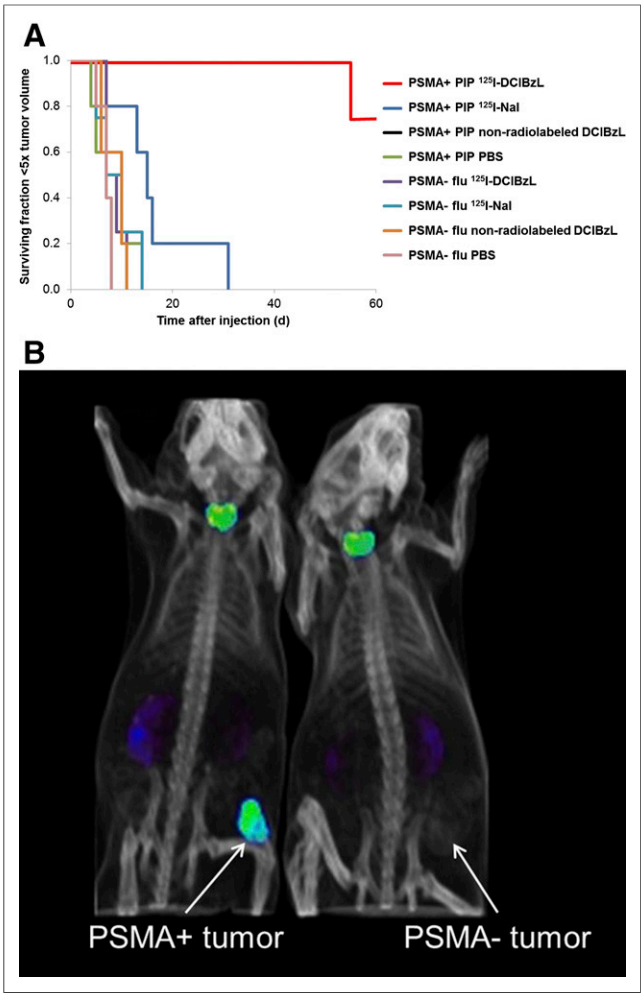

FIGURE 5. (A) Tumor growth delay in nude mice bearing PSMA+ PC3 PIP or PSMA– PC3 flu flank xenografts after treatment with 111 MBq (3 mCi) of ^{125}I-DCIBzL or equal amount of control compounds (n = 5 mice per group; P = 0.002 by log-rank test). (B) Small-animal SPECT/CT maximum-intensity-projection images obtained in 2 of the mice at 24 h after treatment with ^{125}I-DCIBzL. Tumor drug uptake is demonstrated in PSMA+ PC3 PIP tumor (left) but not in PSMA– PC3 flu tumor (right).

which has significant expression of PSMA but a low mitotic index. There are some studies that suggest that Auger emitters may cause cytotoxicity by indirect DNA damage or damage to the plasma membrane or intracellular proteins, but most evidence shows that direct DNA damage predominates (*6,26,31*).

Although the potential for cancer therapy with Auger electrons has long been established, there have been many barriers to successful translation of these therapies (*6,25*). The most-studied Auger therapy has been the thymidine analog ^{125}I-IUdR. That agent is successfully incorporated into DNA, but it is unstable (dehalogenated) when delivered systemically and also causes toxicity due to uptake by normal proliferating cells. Therefore, locoregional delivery, such as intratumoral injection, has been used but with limited scope clinically (*7*). ^{125}I-DCIBzL is relatively stable in vivo after intravenous injection (*8*) and is taken up by PC cells in a highly specific manner. Notably, there was more thyroid uptake of ^{125}I on the SPECT/CT image in Figure 5B than on the SPECT/CT image in the work by Chen et al. (*8*), suggesting possible in vitro radiolysis after synthesis of the larger, more concentrated batch. Radiolysis may be preventable by dilution and addition of free radical scavengers, but stability will need to be confirmed in vitro by high-performance liquid chromatography and in vivo by serial SPECT/CT. Furthermore, long-term follow-up will be needed to assess the safety of systemic delivery. Other targeted Auger therapies have also been developed for breast cancer, ovarian cancer, and lymphoma, but only a few have been tested in vivo, including the radioimmunotherapy ^{111}In-anti-CD74 for B-cell lymphoma (*32,33*).

Because PSMA is overexpressed more than 1,000-fold in human PCs, both in the primary site and in the regional and distant metastases, it has been identified as a therapeutic target for PC (*9,10*). We have tested several lysine-glutamate urea-based scaffolds for targeting PSMA. The ^{125}I-DCIBzL compound has the highest PSMA binding affinity (K_i = 0.01 nM) of all the urea-based PSMA agents we have prepared to date and has shown high and sustained tumor uptake in biodistribution studies (14% injected dose per gram) (*8*). It has also been co-crystallized with PSMA, showing that the bulky iodophenyl moiety is accommodated by a hydrophobic auxiliary subpocket extending beyond the normal binding pocket, and the additional hydrophobic–hydrophobic interactions likely account for the high binding affinity (*34*). Similar agents have been safely administered to patients in low doses for imaging of PC, with successful visualization of small metastases not visible on conventional imaging (*11,12*).

Several systemic RPTs have been approved for PC by the Food and Drug Administration, including the bone-seeking β− emitters ^{153}Sm and ^{89}Sr as well as the α-particle emitter $^{223}RaCl_2$ that has recently demonstrated survival benefit in castrate-resistant PC and is now supplanting the β emitters (*5*). Those agents all successfully target gross PC bone metastases but do not target other sites of disease. Because ^{125}I-DCIBzL has the potential to target all sites, including prostate, pelvic and paraaortic lymph nodes, bone, liver, and lung, it may complement the other modes of RPT, especially for patients with biochemical progression who have no visible bone metastases. Several PSMA-targeted β-emitter RPTs are also being investigated, including the small-molecule ^{131}I-MIP1466, which demonstrated PSMA-specific growth inhibition in tumor xenografts and patients (*35*). The anti-PSMA antibody J591 has been radiolabeled with a variety of β emitters, including ^{177}Lu (*36*). Although well tolerated, that radiolabeled antibody was dose-limited by myelosuppression, particularly thrombocytopenia, which is not expected with small-molecule therapy (due to more rapid clearance) and was not seen in blood counts after treatment with ^{125}I-DCIBzL. As noted above, there are several potential advantages of Auger emitters over β emitters for treatment of micrometastases, but β emitters will likely also have their place for treatment of macroscopic disease.

The in vitro characterization of ^{125}I-DCIBzL was consistent with the proposed mechanism of PSMA-specific uptake and direct DNA damage. The results showed specific cell uptake, DNA damage, and cytotoxicity in PSMA+ PC3 PIP cells but not in PSMA– PC3 flu cells (Figs. 3 and 4; Supplemental Figs. 1 and 2). Treatment with nonradiolabeled DCIBzL showed minimal effect in vitro and in vivo, demonstrating that the PSMA-targeting scaffold itself did not have significant cytotoxic activity. The uptake of ^{125}I-DCIBzL (including all membrane-bound drug) was proportional to extracellular medium concentration (Fig. 3A), suggesting that there was no saturation of the PSMA binding sites (4.9×10^6 sites/cell), possibly due to recycling of PSMA protein. The approximate amount of

DNA damage was also roughly proportional to the concentration within extracellular medium (Fig. 3B), according to number of γH2AX foci. Phosphorylation of histone H2AX is an early focal event in response to DNA double-strand breaks, and this type of DNA damage, if not repaired, results in mitotic catastrophe and cell death (*21*).

We found that clonogenic survival for PSMA+ PC3 PIP cells was roughly an exponential function of extracellular ^{125}I-DCIBzL concentration, as would be expected for radiation-induced cell death. However, when that was modeled using Monte Carlo simulations as a function of estimated dose to the nucleus, it was not perfectly linear on a logarithmic scale (Fig. 4B). On the basis of work by Kassis, Humm, and others, the dose-response curve of Auger emitters should be monoexponential (linear) if close enough to DNA to cause double-strand breaks (*24,26*). We suspect that the modeled dose to the nucleus may be overestimated at high doses, as we assumed 15% perinuclear drug distribution at all drug concentrations. That percentage was based on fluorescent drug distribution after 1-h exposure to YC-36, but at high drug concentrations (18-h exposure to 370 kBq/mL of ^{125}I-DCIBzL), the relative amount of perinuclear drug may be lower due to potential saturation of intracellular PSMA trafficking mechanisms. That highlights the importance of rigorous macro- to microlevel dosimetry for targeted RPTs, especially those with short ranges such as Auger and α emitters (*26,37*). Our ongoing work will model the dosimetry of ^{125}I-DCIBzL at the subcellular, cellular, and organ level for tumor, kidney, and bone marrow. We will correlate kidney dose estimates with long-term nephrotoxicity and histopathology up to 1 y after treatment. We will also correlate tumor dose estimates with tumor response using serial SPECT/CT. SPECT/CT is particularly valuable for quantification of drug delivery, and given the long half-life of ^{125}I, serial SPECT/CT can be used to assess drug kinetics as well as tumor volume measurements over time.

Concerns regarding dosimetry and toxicity of PSMA-targeted agents have been primarily focused on potential nephrotoxicity, because PSMA is physiologically expressed in the renal proximal tubules (*9*). Our previously published biodistribution data for ^{125}I-DCIBzL showed tumor-to-kidney ratios of 0.1 for at least 48 h after injection (*8*). There was less relative kidney uptake in the current SPECT/CT image (Fig. 5B) than the image from the work of Chen et al. (8), but this may be due in part to the later time point after injection, higher PSMA expression in current PC3 PIP tumors, different window/level of images, and different injected dose. In our dose-escalation study, no changes in creatinine were noted 4 d after injection, even at doses of 111 MBq (3 mCi) per mouse. Furthermore, no animals died or lost weight during the 60-d observation period. However, the half-life of ^{125}I-DCIBzL is 59 d and radiation toxicity can manifest long after exposure (often greater than 6 mo for radiation nephropathy). Therefore, as noted above, careful toxicity and dosimetry studies will be required for translation of this agent, with long-term follow-up for 1 y and in larger animals. In addition, given thyroid uptake seen in Figure 5B, drug stability and thyroid toxicity will need to be assessed, and uptake may need to be blocked with pretreatment iodide.

Future work with ^{125}I-DCIBzL will also require testing in additional tumor models and direct comparison with other RPTs. In our flank xenograft model, tumors were treated when only 3–4 mm to mimic the micrometastatic setting; however, this is a limited model of micrometastases, especially with the small scale of a 20-g mouse. Antitumor efficacy needs to be tested in a true metastatic model, and we are currently preparing a PSMA– and luciferase-expressing metastatic PC model for this purpose. We will test in animals with gross metastases as well as those with microscopic metastases not yet visible on imaging.

CONCLUSION

PSMA-targeted RPT with the Auger electron emitter ^{125}I-DCIBzL yielded specific PC cell kill in vitro and in vivo after systemic administration, showing promise for treatment of PC micrometastases. Given kidney uptake of ^{125}I-DCIBzL, long-term nephrotoxicity and dosimetry studies are under way to assess safety for further translation.

DISCLOSURE

The costs of publication of this article were defrayed in part by the payment of page charges. Therefore, and solely to indicate this fact, this article is hereby marked "advertisement" in accordance with 18 USC section 1734. This work was supported by the Maryland Cigarette Restitution Fund Research grant to Johns Hopkins (FY14). It was also supported by NIH CA184228, CA134675, CA183031, CA157542, and EB005324. No other potential conflict of interest relevant to this article was reported.

ACKNOWLEDGMENTS

We thank Dr. Warren Heston for providing the PC3 PIP and PC3 flu cells. Data in this study were presented in part at the 56th Annual Meeting of the American Society for Radiation Oncology; San Francisco; September 2014.

REFERENCES

1. American Cancer Society. *Cancer Facts & Figures 2012.* Atlanta, GA: American Cancer Society; 2012.
2. Previous Version: SEER Cancer Statistics Review, 1975-2009 (Vintage 2009 Populations). Surveillance, epidemiology and end results program website. http://seer.cancer.gov/csr/1975_2009_pops09. Updated August 20, 2012. Accessed July 14, 2015.
3. Antonarakis ES, Feng Z, Trock BJ, et al. The natural history of metastatic progression in men with prostate-specific antigen recurrence after radical prostatectomy: long-term follow-up. *BJU Int.* 2012;109:32–39.
4. Caire AA, Sun L, Ode O, et al. Delayed prostate-specific antigen recurrence after radical prostatectomy: how to identify and what are their clinical outcomes? *Urology.* 2009;74:643–647.
5. Parker C, Nilsson S, Heinrich D, et al. Alpha emitter radium-222 and survival in metastatic prostate cancer. *N Engl J Med.* 2013;369:213–223.
6. Kassis AI. The amazing world of auger electrons. *Int J Radiat Biol.* 2004;80:789–803.
7. Bodei L, Kassis AI, Adelstein SJ, Mariani G. Radionuclide therapy with iodine-125 and other auger-electron-emitting radionuclides: experimental models and clinical applications. *Cancer Biother Radiopharm.* 2003;18:861–877.
8. Chen Y, Foss CA, Byun Y, et al. Radiohalogenated prostate-specific membrane antigen (PSMA)-based ureas as imaging agents for prostate cancer. *J Med Chem.* 2008;51:7933–7943.
9. Silver DA, Pellicer I, Fair WR, Heston WD, Cordon-Cardo C. Prostate-specific membrane antigen expression in normal and malignant human tissues. *Clin Cancer Res.* 1997;3:81–85.
10. Chang SS, Heston WD. The clinical role of prostate-specific membrane antigen (PSMA). *Urol Oncol.* 2002;7:7–12.
11. Barrett JA, Coleman RE, Goldsmith SJ, et al. First-in-man evaluation of 2 high-affinity PSMA-avid small molecules for imaging prostate cancer. *J Nucl Med.* 2013;54:380–387.
12. Cho SY, Gage KL, Mease RC, et al. Biodistribution, tumor detection, and radiation dosimetry of ^{18}F-DCFBC, a low-molecular-weight inhibitor of prostate-specific membrane antigen, in patients with metastatic prostate cancer. *J Nucl Med.* 2012;53:1883–1891.

13. Banerjee SR, Foss CA, Castanares M, et al. Synthesis and evaluation of technetium-99m- and rhenium-labeled inhibitors of the prostate-specific membrane antigen (PSMA). *J Med Chem.* 2008;51:4504–4517.
14. Sobel RE, Sadar MD. Cell lines used in prostate cancer research: a compendium of old and new lines—part 2. *J Urol.* 2005;173:360–372.
15. Sobel RE, Sadar MD. Cell lines used in prostate cancer research: a compendium of old and new lines—part 1. *J Urol.* 2005;173:342–359.
16. Novy Z, Barta P, Mandikova J, Laznicek M, Trejtnar F. A comparison of in vitro methods for determining the membrane receptor expression in cell lines. *Nucl Med Biol.* 2012;39:893–896.
17. Wang X, Ma D, Olson WC, Heston WD. In vitro and in vivo responses of advanced prostate tumors to PSMA ADC, an auristatin-conjugated antibody to prostate-specific membrane antigen. *Mol Cancer Ther.* 2011;10:1728–1739.
18. Govindan SV, Goldenberg DM, Elsamra SE, et al. Radionuclides linked to a CD74 antibody as therapeutic agents for B-cell lymphoma: comparison of Auger electron emitters with beta-particle emitters. *J Nucl Med.* 2000;41: 2089–2097.
19. Chen Y, Pullambhatla M, Banerjee SR, et al. Synthesis and biological evaluation of low molecular weight fluorescent imaging agents for the prostate-specific membrane antigen. *Bioconjug Chem.* 2012;23:2377–2385.
20. Chen Y, Dhara S, Banerjee SR, et al. A low molecular weight PSMA-based fluorescent imaging agent for cancer. *Biochem Biophys Res Commun.* 2009;390: 624–629.
21. Roch-Lefèvre S, Mandina T, Voisin P, et al. Quantification of gamma-H2AX foci in human lymphocytes: a method for biological dosimetry after ionizing radiation exposure. *Radiat Res.* 2010;174:185–194.
22. Franken NA, Rodermond HM, Stap J, Haveman J, van Bree C. Clonogenic assay of cells in vitro. *Nat Protoc.* 2006;1:2315–2319.
23. Agostinelli S, Allison J, Amako K, et al. GEANT4- a simulation toolkit. *Nucl Instrum Meth A.* 2003;506:250–303.
24. Humm JL, Howell RW, Rao DV. Dosimetry of Auger-electron-emitting radionuclides: report no. 3 of AAPM Nuclear Medicine Task Group No. 6. *Med Phys.* 1994;21:1901–1915.
25. Kassis AI. Cancer therapy with Auger electrons: are we almost there? *J Nucl Med.* 2003;44:1479–1481.
26. Kassis AI. Molecular and cellular radiobiological effects of Auger emitting radionuclides. *Radiat Prot Dosimetry.* 2011;143:241–247.
27. Sastry KS. Biological effects of the Auger emitter iodine-125: a review. Report No. 1 of AAPM Nuclear Medicine Task Group No. 6. *Med Phys.* 1992;19:1361–1370.
28. Anilkumar G, Rajasekaran SA, Wang S, Hankinson O, Bander NH, Rajasekaran AK. Prostate-specific membrane antigen association with filamin A modulates its internalization and NAALADase activity. *Cancer Res.* 2003;63: 2645–2648.
29. Rajasekaran SA, Christiansen JJ, Schmid I, et al. Prostate-specific membrane antigen associates with anaphase-promoting complex and induces chromosomal instability. *Mol Cancer Ther.* 2008;7:2142–2151.
30. Balagurumoorthy P, Xu X, Wang K, Adelstein SJ, Kassis AI. Effect of distance between decaying ^{125}I and DNA on Auger-electron induced double-strand break yield. *Int J Radiat Biol.* 2012;88:998–1008.
31. Pouget JP, Santoro L, Raymond L, et al. Cell membrane is a more sensitive target than cytoplasm to dense ionization produced by auger electrons. *Radiat Res.* 2008;170:192–200.
32. Costantini DL, Bateman K, McLarty K, Vallis KA, Reilly RM. Trastuzumab-resistant breast cancer cells remain sensitive to the auger electron-emitting radiotherapeutic agent ^{111}In-NLS-trastuzumab and are radiosensitized by methotrexate. *J Nucl Med.* 2008;49:1498–1505.
33. Michel RB, Rosario AV, Andrews PM, Goldenberg DM, Mattes MJ. Therapy of small subcutaneous B-lymphoma xenografts with antibodies conjugated to radionuclides emitting low-energy electrons. *Clin Cancer Res.* 2005;11:777–786.
34. Barinka C, Byun Y, Dusich CL, et al. Interactions between human glutamate carboxypeptidase II and urea-based inhibitors: structural characterization. *J Med Chem.* 2008;51:7737–7743.
35. Hillier S, Rubino K, Maresca K, et al. [^{131}I]MIP-1466, a small molecule prostate-specific membrane antigen (PSMA) inhibitor for targeted radiotherapy of prostate cancer [abstract]. *J Nucl Med.* 2012;53(suppl 1):170.
36. Tagawa ST, Beltran H, Vallabhajosula S, et al. Anti-prostate-specific membrane antigen-based radioimmunotherapy for prostate cancer. *Cancer.* 2010;116(4, suppl): 1075–1083.
37. Hobbs RF, Song H, Huso DL, Sundel MH, Sgouros G. A nephron-based model of the kidneys for macro-to-micro alpha-particle dosimetry. *Phys Med Biol.* 2012;57:4403–4424.